

# Pair-wise, deformable Mirror, image plane-based diversity electric field estimation for high contrast coronagraphy

Amir Give'on<sup>a</sup>, Brian D.Kern<sup>a</sup>, Stuart Shaklan<sup>a</sup>,

<sup>a</sup>Jet Propulsion Laboratory, California Institute of Technology, Pasadena, California, USA

## ABSTRACT

In this paper we describe the complex electric field reconstruction from image plane intensity measurements for high contrast coronagraphic imaging. A deformable mirror (DM) surface is modified with pairs of complementary shapes to create diversity in the image plane of the science camera where the intensity of the light is measured. Along with the Electric Field Conjugation correction algorithm, this estimation method has been used in various high contrast imaging testbeds to achieve the best contrasts to date both in narrow and in broad band light. We present the basic methodology of estimation in easy to follow list of steps, present results from HCIT and raise several open questions we are confronted with using this method.

**Keywords:** high contrast imaging, wavefront estimation

## 1. INTRODUCTION

Recent high-contrast coronagraphic imaging techniques have led to the laboratory demonstration of starlight suppression with sensitivity adequate to detect earth-like planets around nearby stars.<sup>1</sup> These results were achieved in monochromatic light, narrow band light (2%) and broadband light (up to 20%) using the Electric Field Conjugation (EFC) algorithm along with the image plane-based electric field estimation that is described in this paper, applied with various types of coronagraphs.<sup>1-7</sup>

This estimation technique has been developed for a family of wavefront correction algorithms such as the EFC,<sup>1</sup> Energy Minimization<sup>8</sup> and Stroke Minimization,<sup>9</sup> all requiring an estimate of the complex valued wavefront in the image plane. The EFC algorithm and the other image plane intensity measurements based correction algorithms require an estimate of the complex field in the science camera image plane in order to determine the commands of the deformable mirror to minimize the total intensity of light in a predetermined region in the image plane.<sup>1</sup> The high contrast needed for Earth-like planet detection determines the requirements from the coronagraph and correction system.

In order to avoid non-common path errors this estimation technique uses the deformable mirror (DM) to perturb the electric field (EF) at the DM's plane rather than using an additional optical path with an interferometer.<sup>10</sup> Moreover, a typical high contrast imaging coronagraph has masks along its optical path, as such, methods that require both forward and backward numerical propagation of the EF through the system suffer from non-uniqueness effects and/or large errors due to edge effects. The estimation method described in this paper uses only forward propagation of the EF through the coronagraph.

Since the measured quantity at the science camera is the intensity of the EF, a perturbation of the EF is needed in order to retrieve the phase information that was lost. In the case presented here, we take a series of intensity measurements at the science camera plane with different changes to the DM surface (these changes to the EF are referred to as "probes") and estimate the EF at the science camera image plane. The modulation scheme we describe in this paper is a sequence of DM shapes with accompanying intensity measurements, each intended to exploit the nonlinear relationship of the intensity measurements to the additive EF due to the change in the DM, which then allow determination of the EF before the probes were applied. Analogously to a phase-shifting interferometer, taking four intensity measurements with varying phase by multiples of  $e^{i\pi/2}$  would allow unambiguous determination of the complex EF in the image plane from intensity measurements alone for every point in the plane simultaneously.<sup>11</sup>

The baseline method of this estimation technique uses 5 intensity measurements. The first is the intensity measurement of the EF in its current state of the DM along with 2 pairs of intensity measurement. Each pair

consists of a positive and negative change to the DM (same change). The 2 pairs of images are used algebraically to produce an estimate of the complex EF before the probes were applied. The 5th image, without the probes, is used to determine the incoherent light (when present) and the amplitude of the probes.

## 2. PAIRWISE ESTIMATION

### 2.1 The intensity measurements model

For a general coronagraphic system, we define two planes of interest. The first is the plane of the DM, the second is the plane of the science camera. With respect to the scope of this paper, the plane of the DM is thought of the plane where changes can be made, and the plane of the science camera is the plane where measurements are taken and the plane where the EF is to be estimated. Assume the science camera measures the total intensity of light in an image plane we may write

$$I = |E|^2 + I_{\text{inc}}, \quad (1)$$

where  $I$ ,  $E$ , and  $I_{\text{inc}}$  are all functions of two spatial variables in the image plane,  $(x, y)$ , and  $E$  is complex-valued. Let  $E$  be defined as the coherent part of the EF in the image plane and  $I_{\text{inc}}$  be defined as the intensity of the incoherent part of the EF in the image plane. A deformable mirror is part of a coronagraph optical train, which can be represented by

$$E = C \left[ \tilde{E} \right], \quad (2)$$

where  $\tilde{E}$  is a complex-valued function of two spatial variables in the DM plane,  $(\xi, \eta)$  that represents the complex electric field including the current shape of the DM, and  $C$  is a linear operator (could be a series of Fourier transforms but typically is the propagation of electric field between the DM plane and the camera image plane, including stops and occulters along the optical path to the final image plane). Let  $I_0$  be defined as the measured intensity in the image plane for a given DM settings, that is,

$$I_0 = \left| C \left[ \tilde{E}_T \right] \right|^2 + I_{\text{inc}}. \quad (3)$$

The Electric Field Conjugation correction algorithm (and other image plane-based correction algorithms mentioned above) requires an estimate of  $E_T = C \left[ \tilde{E}_T \right]$  in regions of  $(x, y)$  that are faint (in intensity) relative to the core of an unocculted PSF, maybe by factors of  $10^{-10}$ . In practice,  $\tilde{E}_T$  is not known to  $10^{-5}$  precision, which is needed to bring the contrast in the desired region down to  $10^{-10}$  with respect to the core. Let  $\tilde{E}_T = \tilde{E}_0 + \delta\tilde{E}$ , where  $\tilde{E}_0$  represents the best estimate we have for,  $\tilde{E}_T$ , the EF in the DM plane and  $\delta\tilde{E}$  is the error in this estimate. In order to estimate  $E_T$ , additional measurements are needed with some modulation of the to-be estimated signal. We do so by modulating the DM with small changes. Let  $\Delta\psi$  be a real-valued function of DM spatial variables expressed in radians, and will be assumed to be small everywhere compared to 1 rad, then the intensity in the image plane for the “probed” system can be modeled as

$$\begin{aligned} I_p &= \left| C \left[ \tilde{E}_T e^{\Delta\psi} \right] \right|^2 + I_{\text{inc}} \\ &\approx \left| E_T + iC \left[ \tilde{E}_T \Delta\psi \right] \right|^2 + I_{\text{inc}}, \end{aligned} \quad (4)$$

where we have used the linear approximation to  $e^{i\Delta\psi_i}$  for small  $\Delta\psi_i$ .  $\Delta\psi$  varies as different voltages are commanded on the DM actuators, while  $\tilde{E}_T$  is unchanged by DM voltages. The pairwise estimation uses DM modulation with opposite phase terms,  $\Delta\psi_i$  and  $-\Delta\psi_i$  for the two components (+ and -) of each pair of probed images. In the base method we use 2 such pairs, for  $i = 1, 2$ :

$$\begin{aligned}
I_i^+ &= \left| E_T + iC \left[ \tilde{E}_T \Delta\psi_i \right] \right|^2 + I_{inc} \\
I_i^- &= \left| E_T - iC \left[ \tilde{E}_T \Delta\psi_i \right] \right|^2 + I_{inc},
\end{aligned} \tag{5}$$

giving the 5 intensity measurements model (including the measurement of  $I_0$ ) for the estimation process:

$$\begin{aligned}
I_0 &= |E_T|^2 + I_{inc} \\
I_1^+ &= \left| E_T + iC \left[ \tilde{E}_T \Delta\psi_1 \right] \right|^2 + I_{inc} \\
I_1^- &= \left| E_T - iC \left[ \tilde{E}_T \Delta\psi_1 \right] \right|^2 + I_{inc} \\
I_2^+ &= \left| E_T + iC \left[ \tilde{E}_T \Delta\psi_2 \right] \right|^2 + I_{inc} \\
I_2^- &= \left| E_T - iC \left[ \tilde{E}_T \Delta\psi_2 \right] \right|^2 + I_{inc}.
\end{aligned} \tag{6}$$

Given an estimate for  $E_T$ , this set of equations can be used to quantify the agreement of the model with the measurements and the reconstructed EF.

## 2.2 The estimation algorithm

In order to estimate  $E_T$  we further approximate the effect of the DM change in the image plane and notate

$$\begin{aligned}
\Delta p_i &= C \left[ \tilde{E}_T \Delta\psi_i \right] \\
&\approx C \left[ \tilde{E}_0 \Delta\psi_i \right],
\end{aligned} \tag{7}$$

as the linearized model of the approximated complex-valued probe amplitude in the image plane, defined for every  $(x, y)$ . In practice, it is possible to determine the absolute value of  $\Delta p_i$  from noting that

$$|\Delta p_i| = \sqrt{\frac{I_i^+ + I_i^-}{2} - I_0}, \tag{8}$$

and its approximated phase is determined by propagating  $\Delta\psi_i$  through the approximated model as in Eq. 7. We then examine the differences between the pairs of intensity measurements

$$\begin{aligned}
\delta_i &= (I_i^+ - I_i^-) / 2 \\
&= -2 \operatorname{Re} \{ E_T \} \operatorname{Im} \{ \Delta p_i \} + 2 \operatorname{Im} \{ E_T \} \operatorname{Re} \{ \Delta p_i \}.
\end{aligned} \tag{9}$$

To convert the  $\delta_1$  and  $\delta_2$  measurements into a complex estimate of  $E_T$ , for every  $(x, y)$  point we solve

$$\begin{bmatrix} \delta_1 \\ \delta_2 \end{bmatrix} = 2 \begin{bmatrix} -\operatorname{Im} \{ \Delta p_1 \} & \operatorname{Re} \{ \Delta p_1 \} \\ -\operatorname{Im} \{ \Delta p_2 \} & \operatorname{Re} \{ \Delta p_2 \} \end{bmatrix} \begin{bmatrix} \operatorname{Re} \{ E_T \} \\ \operatorname{Im} \{ E_T \} \end{bmatrix}. \tag{10}$$

This allows a full determination of  $E_T$  for every  $(x, y)$  point simultaneously, using only the differences in the four intensity measurements  $I_1^+$ ,  $I_1^-$ ,  $I_2^+$ ,  $I_2^-$  and the measurement of the original EF intensity,  $I_0$ . These differences,  $\delta_i$ , are on the order of  $|E_0 \Delta p_i|$ .

It is possible to use more pairs of probes to reduce estimation errors. In this case, Eq. 10 expands to

$$\begin{bmatrix} \delta_1 \\ \delta_2 \\ \vdots \\ \delta_N \end{bmatrix} = 2 \begin{bmatrix} -\text{Im} \{ \Delta p_1 \} & \text{Re} \{ \Delta p_1 \} \\ -\text{Im} \{ \Delta p_2 \} & \text{Re} \{ \Delta p_2 \} \\ \vdots & \vdots \\ -\text{Im} \{ \Delta p_N \} & \text{Re} \{ \Delta p_N \} \end{bmatrix} \begin{bmatrix} \text{Re} \{ E_T \} \\ \text{Im} \{ E_T \} \end{bmatrix} \quad (11)$$

and can be solved by inverting the  $N \times 2$  matrix per pixel using singular value decomposition. The condition for existence of a solution per pixel in both the case of 2 pairs or  $N$  pairs is that the rank of this matrix is 2. This is accomplished by the specific probe shapes applied to the DM discussed in the next section.

### 3. LAB RESULTS

Calibration errors on the DM lead to relatively simple probe patterns. In practice, we choose a pattern on the DM that gives near-uniform additive amplitude in rectangular regions in the image plane (see Fig. 1). In theory, the patterns can be altered to better match the intensity pattern of  $I_0$  in the region of interest and even take into account the transfer function of the DM. For the purpose of presenting the basic estimation algorithm we are showing the simplest pattern. This pattern, expressed in  $(x, y)$  DM coordinates (pupil-plane coordinates), is

$$\psi(x, y; \theta) = P \text{sinc}(\Delta\xi x) \text{sinc}(\Delta\eta y) \sin(2\pi\xi_c x + \theta), \quad (12)$$

where  $P$  is the probe amplitude,  $\Delta\xi$  is the  $\xi$ -width of the rectangular probe region in the image plane,  $\Delta\eta$  is the  $\eta$ -height of the rectangular probe region,  $\xi_c$  is the center of the rectangular region, and  $\theta$  is the probe spatial phase. Here,  $\text{sinc}(s) = \sin(\pi s)/(\pi s)$ . The overly simplistic conceptual effect of these probes in the image plane is to add a uniform complex amplitude electric field component (spatially uniform in both phase and amplitude) to the existing image plane electric field, over two symmetric rectangular regions of size  $\Delta\xi \times \Delta\eta$ , centered at  $(-\xi_c, 0)$  and  $(\xi_c, 0)$ . Typically, we use a rectangle that covers  $4 < \xi/(\lambda f/D) < 10$ ,  $-10 < \eta/(\lambda f/D) < 10$  (and its symmetric pair).. The phases of the two rectangles are negatives of one another (the additive field is Hermitian). A more accurate representation (the one used in the actual estimation below) requires consideration of the coronagraph components and the DM's influence function transfer functions. Figure 1 shows the 4 DM surface changes used and their corresponding complex-valued effect in the image plane.

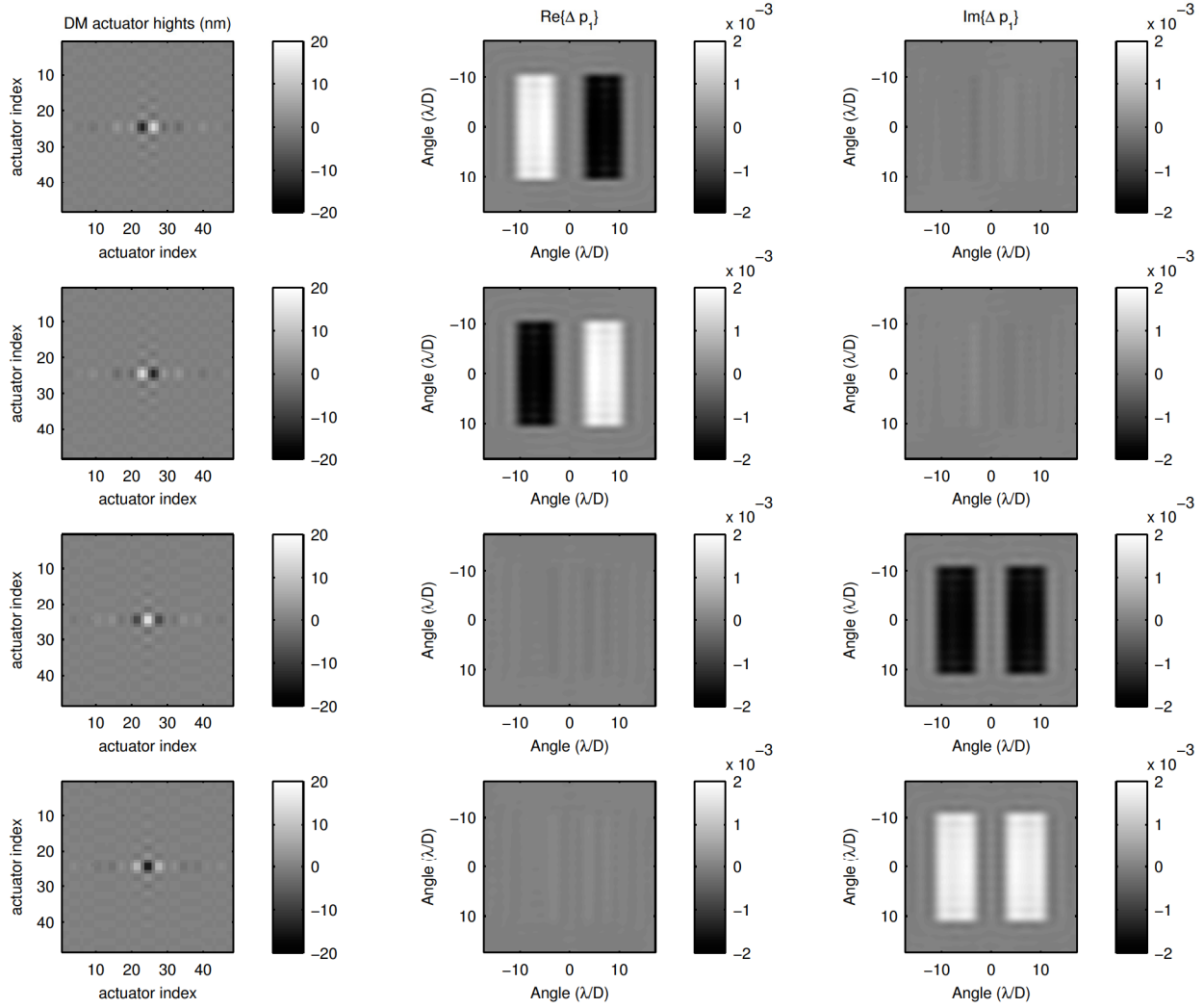


Figure 1. The four different DM patterns and their corresponding expected changes in EF in the image plane (see Eq. 12). The left column shows the actuator hights commands in nanometers, the middle and right column show the real and imaginary parts, respectively, of the expected (from simulation) change in EF in contrast units due to the change in the DM surface.

As seen in the figure, the patterns were chosen such that the diversity per pixel is maximized between real and imaginary parts “excitation”, maximizing diversity in order to be more robust to errors in the model and errors due to measurement. In practice, this translates to a rank of 2 for the matrices in equations 10 or 11.

Applying these changes to the DM produces the intensity measurements shown in Fig. 2.

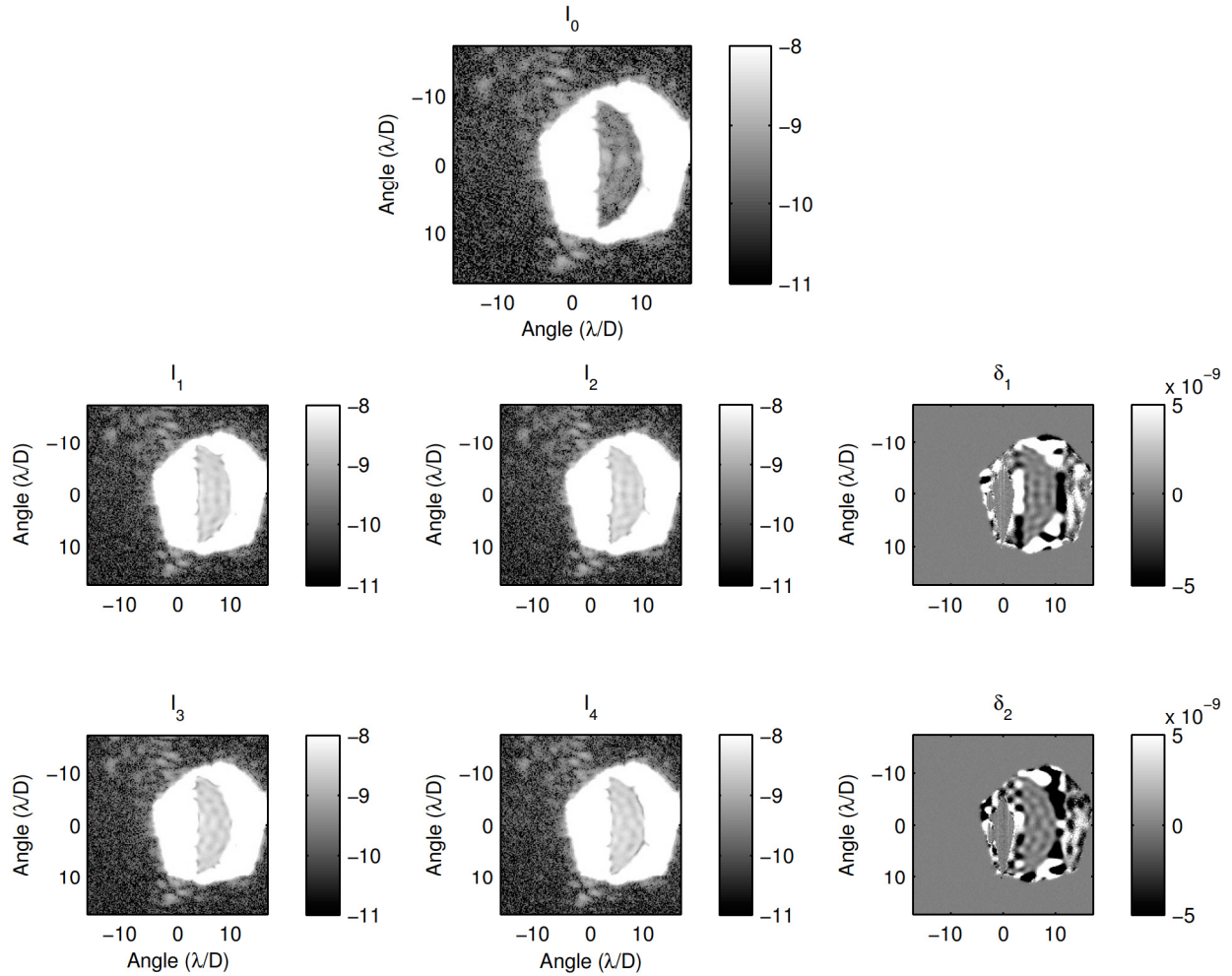


Figure 2. Top image shows the intensity measurement in the image plane, corresponding to Eq. 3. Note that an image plane mask was placed right in front of the CCD camera to block some of the light. The second and third rows show the intensity measurements of the probed systems where the DM was changed according to Eq. 4. The right column in these two rows shows the differenced images according to Eq. 9.

As seen in figure 2, the effect of the changes to the DM that are described in Eq. 12 and shown in Fig. 1 is to modulate the light in the region of interest such that the difference in intensity measurements between probed pairs provides the diversity needed for estimation of the EF in the un-probed image.

Figure 3 shows a model validation of the probes intensity before the replacement of the probe amplitude with measured data according to equation 8. The probes amplitudes were calculated first by the model of the DM surface change and propagation through the model of the coronagraph (equation 7) then calculated from the intensity measurements as described in equation 8.

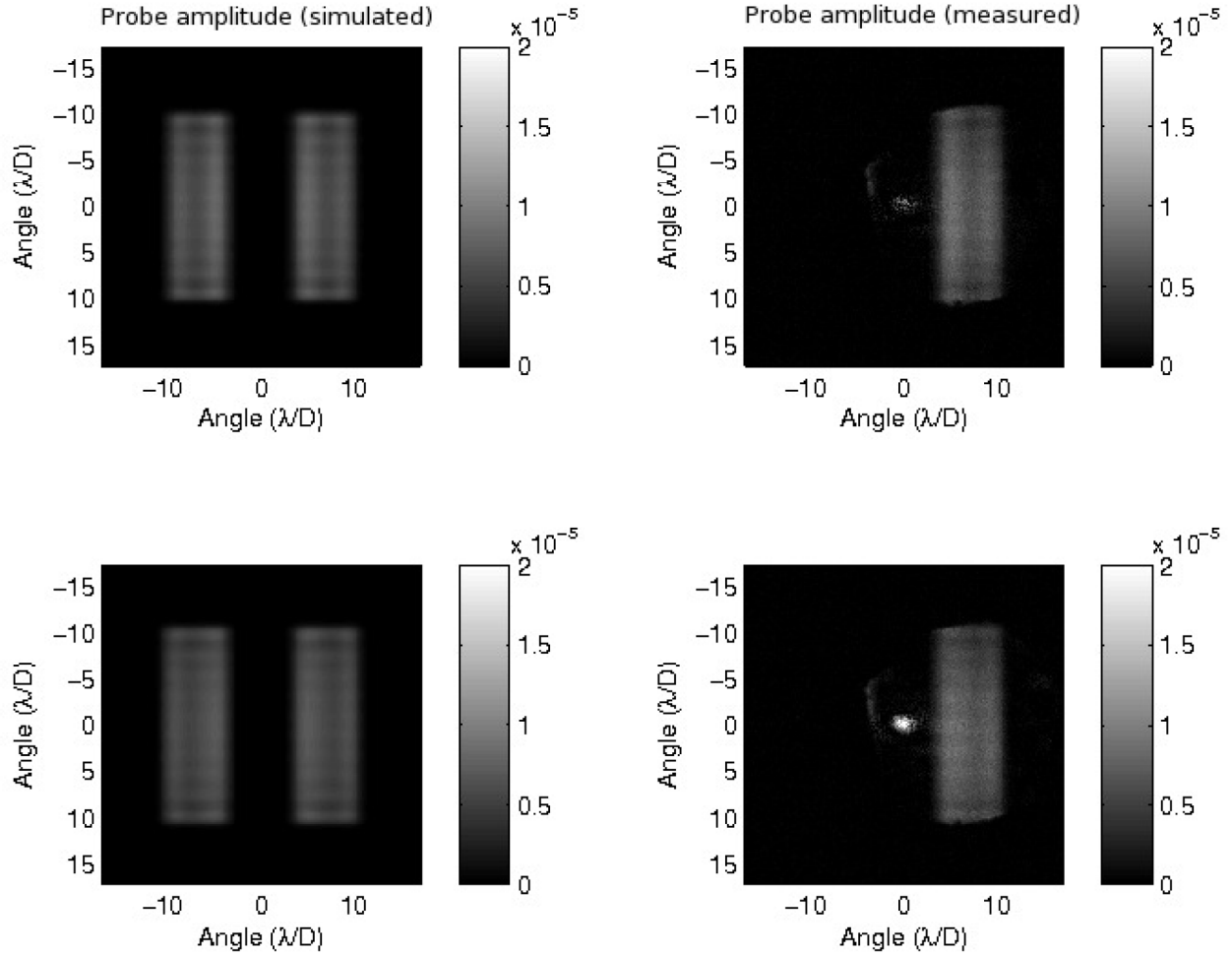


Figure 3. This image compares the expected (simulated) absolute value of the EF due to the DM changes (left column) to that measured (right column). The comparison is done following Eq. 8. Note that the intensity measurements are taken with an image plane mask that lets light through on only one side of the image plane.

As seen in the figure, the model of the probes amplitude agrees both in magnitude and in morphology across the region of interest. In order to make the estimation set of equations fully determined (in this case, five equations and five quantities calculated), the amplitude of the probes in equation 6 is replaced on a point by point basis with the measured amplitude following equation 8.

In general, only one side of the image plane is of interest at any given time, while the opposite side remains at a contrast limited by the wavefront amplitude errors in the system (between  $10^{-6}$  and  $10^{-7}$  on HCIT). Taking images at each of the probe DM settings allows Eq. 10 to deliver an estimate of the complex image plane electric field. Figure 4 shows the result of estimating the EF at one of the iterations of EFC on HCIT.

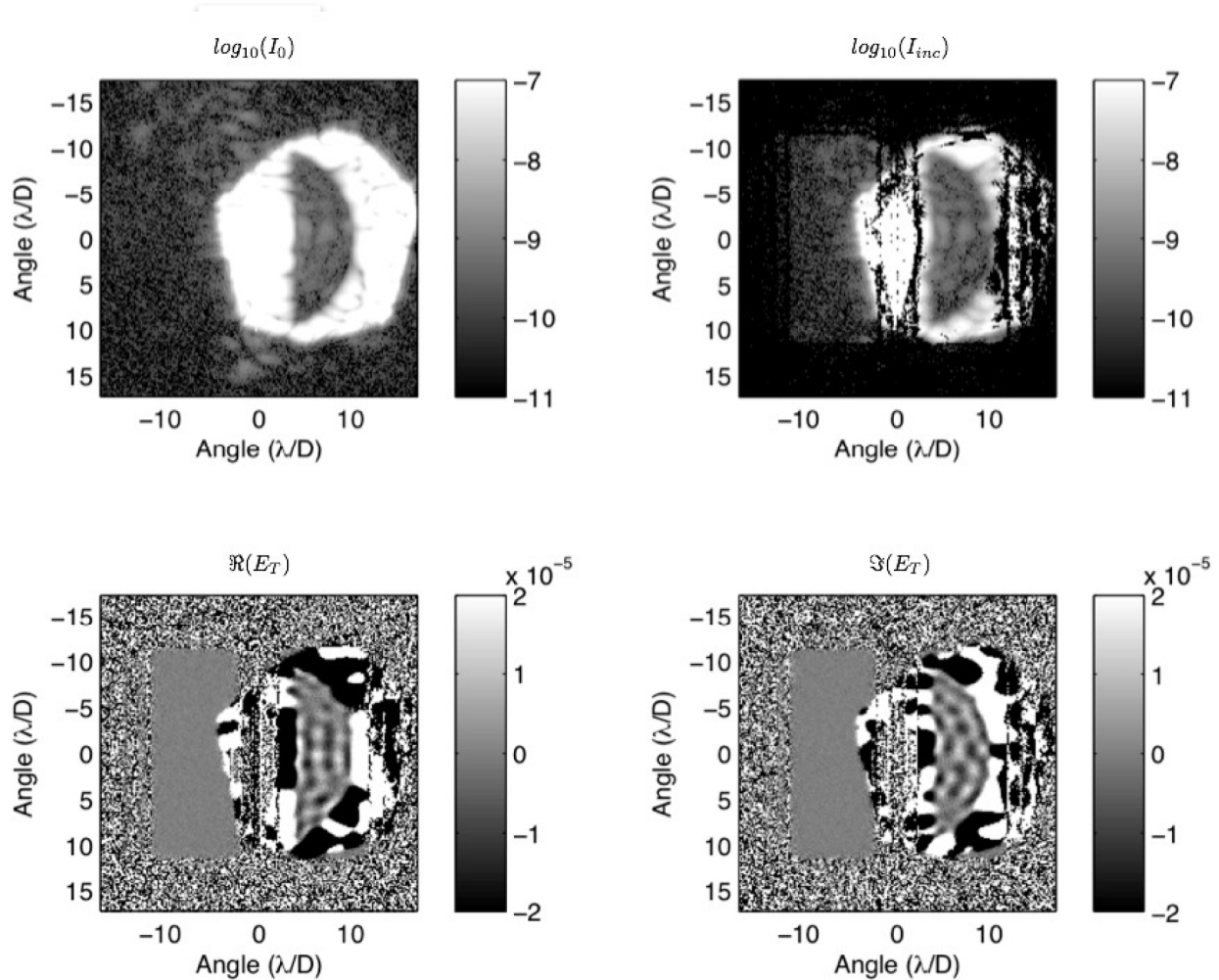


Figure 4. This figure shows the result of estimating the complex EF showing the different quantities in the first line of equation (set) 6. The result of the reconstruction is to decompose the real and imaginary parts of  $E_T$  and solving for the incoherent light, both, per pixel within the region of interest.

The probes intensities were chosen (by setting up the amplitude of the change in the surface of the DM) to modulate the light within the region of interest. In the case shown in the figure, this region is  $4 < \xi/(\lambda f/D)$  and  $\rho/(\lambda f/D) < 10$ , where  $\rho = \sqrt{\xi^2 + \eta^2}$ .

#### 4. LIMITATIONS AND FUTURE WORK

One of the greatest challenges facing those using wavefront reconstruction techniques which use the deformable mirror to provide the diversity for estimation, such as the method described here, is distinguishing “real” incoherent light from the quantity left from equation 1 after the coherent part was estimated. Clearly, any errors in estimating  $E$  in equation 1 would give rise to an error in  $I_{inc}$ . In order to demonstrate and depict the problem, figure 5 shows a general case of running EFC to correct for amplitude and phase of the EF on one side of the image plane, in a region similar to that shown in figure 4. The quantities plotted are the average over the D-shape regions of the intensities of both the coherent part and the incoherent part. It is important to note that in this run, the exposure time was increased once at the 8th iteration (as shown in the plot).

One unsolved question with regards to this estimation method (and this is observed in all runs and in other testbeds) is the change in incoherent light intensity throughout the iterations. Figure 5 can be divided in this

respect to three regions (as seen in the plot). In the first region, the incoherent light stays at 1/10 of the coherent light level. In region 2, the coherent light reduces at a faster rate than the incoherent light does. Region 3 is when the coherent light continues to decline while the incoherent light converges to a relatively constant level. This behavior is yet to be explained and repeats itself to some degree in all runs.

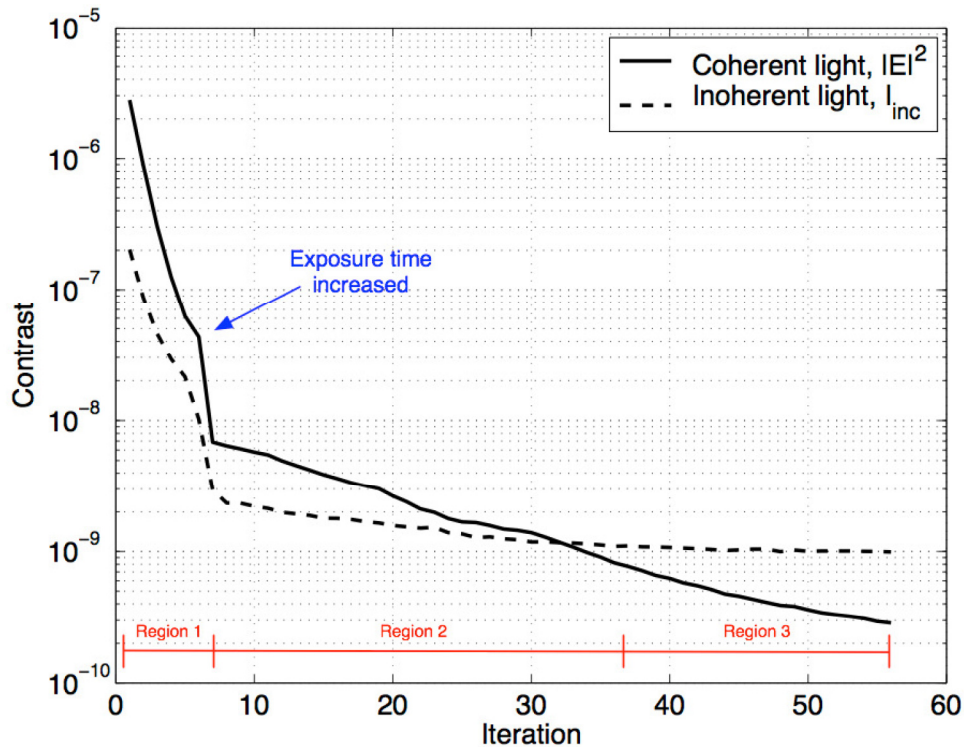


Figure 5. Coherent versus incoherent light throughout several iterations. The plot shows the evolution of the two quantities,  $E_T$  and  $I_{inc}$  in equation 6 as the contrast in the dark zone converges.

The conditions under which light can appear to be “uncontrollable” (DM modulation does not have an interferometric signature on intensities) can be categorized as insufficient resolution in a number of ways,<sup>12</sup> namely spatially unresolved (variations in wavefront amplitude on smaller scale than the camera pixel sampling), temporally unresolved (changes in the wavefront amplitude over time that are faster than the sequence of images taken for the estimation), spectrally unresolved (OPD’s exceed coherence length of source), unresolved polarization states, measurement noise and lastly, modeling error that will print through the estimation and give a erroneous result for the difference between the measured intensity and the intensity of the coherent light.

## 5. SUMMARY

We have presented a DM diversity based estimation technique for reconstruction of the complex EF in the image plane based on intensity measurements. The method uses a typical diversity methodology with a unique way of achieving the diversity. In this case, the diversity in the EF is done by changing the DM, using pairs of perturbation patterns (“probes”). This paper described the complete details of how to solve for the EF and proposed various ways to validate the model used. Without an independent measurement of the EF, it is impossible to quantify the accuracy of each reconstruction. However, since this method is used in conjunction with the EFC correction algorithm to sub-nanometer level of correction, it is considered the best estimation technique to date. That said, there are several open questions that are presented in this paper regarding the relationship between coherent and incoherent light throughout correction runs.

## ACKNOWLEDGMENTS

This work was carried out at the Jet Propulsion Laboratory, California Institute of Technology, under contract with the National Aeronautics and Space Administration.

## REFERENCES

- [1] Amir Give'on, Brian Kern, Stuart Shaklan, Dwight C. Moody, Laurent Pueyo *Demonstration of a symmetric dark hole with a stroke-minimizing correction algorithm*. Proc. SPIE 6691, 66910A (2007).
- [2] Tyler D. Groff, Alexis Carlotti, and N. Jeremy Kasdin *Progress on broadband control and deformable mirror tolerances in a 2-DM system*. Proc. SPIE 7731, 77314S (2010).
- [3] Brian Kern, Ruslan Belikov, Amir Give'on, Olivier Guyon, Andreas Kuhnert, Marie B. Levine-West, Ian C. McMichael, Dwight C. Moody, Albert F. Niessner, Laurent Pueyo, Stuart B. Shaklan, Wesley A. Traub, and John T. Trauger *Phase-induced amplitude apodization (PIAA) coronagraph testing at the High Contrast Imaging Testbed*. Proc. SPIE 7440, 74400H (2009).
- [4] Dimitri Mawet, John T. Trauger, Eugene Serabyn, Dwight C. Moody, Jr., Kurt M. Liewer, John E. Krist, David M. Shemo, and Nada A. O'Brien *Vector vortex coronagraph: first results in the visible*. Proc. SPIE 7440, 74400X (2009).
- [5] Olivier Guyon, James R. P. Angel, Dana Backman, Ruslan Belikov, Donald Gavel, Amir Giveon, Thomas Greene, Jeremy Kasdin, James Kasting, Marie Levine, Mark Marley, Michael Meyer, Glenn Schneider, Gene Serabyn, Stuart Shaklan, et al. *Pupil mapping Exoplanet Coronagraphic Observer (PECO)*. SPIE 7010, 70101Y (2008).
- [6] Ruslan Belikov, Amir Give'on, Brian Kern, Eric Cady, Michael Carr, Stuart Shaklan, Kunjithapatham Balasubramanian, Victor White, Pierre Echternach, Matt Dickie, John Trauger, Andreas Kuhnert, and N. Jeremy Kasdin *Demonstration of high contrast in 10% broadband light with the shaped pupil coronagraph*. Proc. SPIE 6693, 66930Y (2007).
- [7] Sandrine J. Thomas, Amir A. Give'on, Daren Dillon, Bruce Macintosh, Donald Gavel, and Remi Soummer *Laboratory test of application of electric field conjugation image-sharpening to ground-based adaptive optics*. Proc. SPIE 7736, 77365L (2010).
- [8] Borde P. J. and Traub W. A., *High-contrast imaging from space: Speckle nulling in a low aberration regime*. Applied Physics Journal, 638, February 2006.
- [9] Laurent A. Pueyo, Jason D. Kay and N. Jeremy Kasdin *Demonstration of a symmetric dark hole with a stroke-minimizing correction algorithm*. Proc. SPIE 7209, 72090G (2009).
- [10] Laurent Pueyo, Kent Wallace, Mitchell Troy, Rick Burruss, Bruce Macintosh, Remi Soummer *Advanced static speckle calibration for exoplanet imaging*. Proc. SPIE 7209, 72090G (2009).
- [11] Katherine Creath *Phase-shifting speckle interferometry*. Appl. Opt. 24, 3053-3058 (1985).
- [12] Brian Kern, Olivier Guyon, Amir Giveon, Andreas Kuhnert, Albert Niessner *Laboratory Testing of a Phase Induced Amplitude Apodization (PIAA) Coronagraph*. Proc. SPIE 8151 (2011).